Analytical Calculation of Fields, Forces and Losses of a Radial Magnetic Bearing With a Rotating Rotor Considering Eddy Currents

Markus Ahrens
International Center for Magnetic Bearings
ETH Zurich, Switzerland

Ladislav Kučera
International Center for Magnetic Bearings
ETH Zurich, Switzerland

Abstract: This paper presents an analytical model of a radial magnetic bearing with which magnetic fields, forces and losses are calculated. When an unlaminated rotor rotates in a radial magnetic bearing, eddy currents are caused to flow inside the conducting material of the rotor. These eddy currents change the magnetic field of the radial bearing and, therefore, the forces on the rotor depend on the eddy currents. Additionally to the levitation force, a tangetial force acts on the rotor. This tangential force causes a retardation torque which has been measured for many magnetic bearing systems. When the rotor is excited, the tangential force additionally leads to a cross coupling between the x and y axis which may destabilize the system. It will be shown that the forces and losses of a radial bearing depend on the pole configuration. It can be seen that the configuration NSNS has smaller losses than NNSS. The analytical results presented in this paper correspond with measurements [8].

Nomenclature

b	length of a radial bearing
$\boldsymbol{B}$	magnetic flux density
$\boldsymbol{E}$	electric field strength
F	force
$\boldsymbol{H}$	magnetic field strength
$\boldsymbol{J}$	current density
R	radius of the radial bearing
U	circumference of the rotor
$\boldsymbol{v}$	velocity
x, y, z	coordinate directions
δ	penetration depth
Δ	air gap
Ω	rotational speed
σ	conductivity
μ	permeability

1 Introduction

Normally aerodynamic drag causes the largest loss in a rotating rotor but under vacuum condition eddy current losses are dominant. Due to the reduced heat transfer in a vacuum, an adequate model of eddy current losses is desirable.

An analytical solution has some advantages compared with numerical results achieved with Finite Element analysis because it gives a better insight into the problem. Furthermore, numerical calculations for radial bearings often do not succeed. In order to achieve a correct and stable numerical result a small grid width and a large number of elements is necessary. For higher velocities (rotational speeds) the number of elements increases rapidly and it may reach computational limits [1], [3].

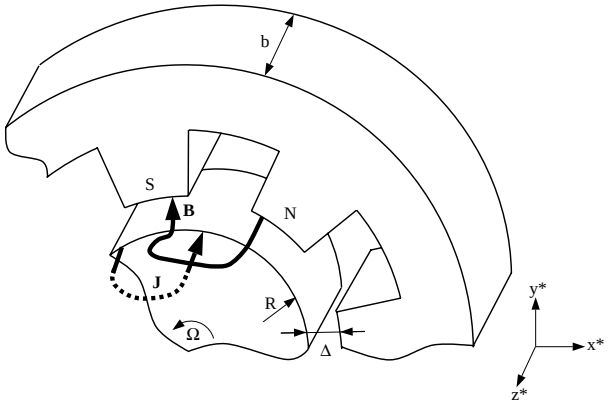

Figure 1: Cross-section of a radial magnetic bearing

Changing magnetic fields inside conducting materials cause eddy currents to flow. When a rotor rotates in a radial magnetic bearing the direction of magnetic flux density in the air gap changes from $+\hat{B}_0$ (north pole N) to $-\hat{B}_0$ (south pole S). Outside of the pole regions the magnetic flux density is zero. This changing magnetic field therefore induces eddy currents in the ferromagnetic and electrically conductive rotor. These currents respectively induce magnetic fields, which change the original

field.

The model in this paper is two dimensional and, therefore, it can only be used for unlaminated rotors. The magnetic flux density distribution is approximated with Fourier series. With this model the magnetic fields, forces and losses are calculated. The results achieved in this paper can be verified with measurements of the retardation torque and the eddy current losses.

The model for a radial magnetic bearing with eddy currents is similar to models used for the analysis of magnetically levitated vehicles (MAGLEV) but the boundary conditions are different [13]. A more adequate approach, which is also used in this paper, is given in [9] and [2].

2 Model

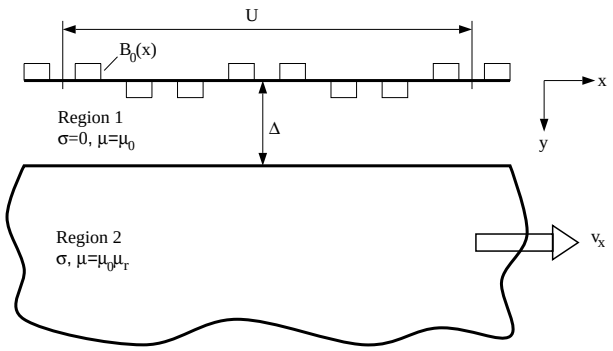

Figure 2: A moving conducting medium under the applied flux density B_0.

For the following calculations, all magnetic poles of the radial bearing are assumed to be identical. In order to solve Maxwell's equations it is necessary to define appropriate boundary conditions.
The magnetic flux density at the boundary between the stator and the air gap is assumed to be constant ($\pm\hat{B}_0$) and the applied flux density is periodic. Conductivity and permeability are assumed to be constant. Saturation and hysteresis effects are neglected.
Another assumption is that the magnetic field and the induced currents tend to concentrate at the surface of the rotor. When the penetration depth δ of the magnetic field is small compared with the diameter of the rotor the error using cartesian coordinates (x, y) instead of cylindrical coordinates (r, φ) is small.

$$\delta = \sqrt{\frac{2}{\sigma\mu\Omega}} \tag{1}$$

The rotational speed Ω can then be replaced by the velocity $v_x = \Omega/R$. Hence the problem of a rotor rotating in radial bearings can be approximated by a semi-infinite conducting plate moving under magnetic poles.

3 Fourier Approximation

In the first step, the flux density B_0 will be approximated by a Fourier series (see [6]).

$$B_0 = \sum_{n=1}^{\infty} A_n \cos(k_n x) + B_n \sin(k_n x) \tag{2}$$

$$= \sum_{n=1}^{\infty} \frac{A_n + iB_n}{2} \mathrm{e}^{ik_n x} + \frac{A_n - iB_n}{2} \mathrm{e}^{-ik_n x} \tag{3}$$

$$= \sum_{n=1}^{\infty} C_n \mathrm{e}^{ik_n x} + \bar{C}_n \mathrm{e}^{-ik_n x} \tag{4}$$

with $k_n = 2\pi n/U = n/R$.

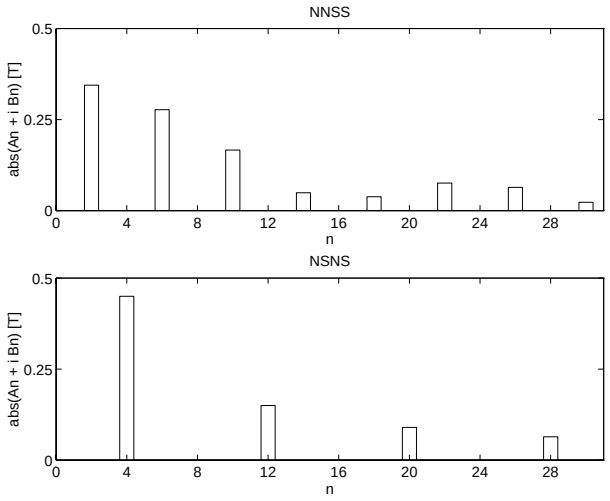

Figure 3: Fourier series of the two radial magnetic bearing configurations (NNSS and NSNS).

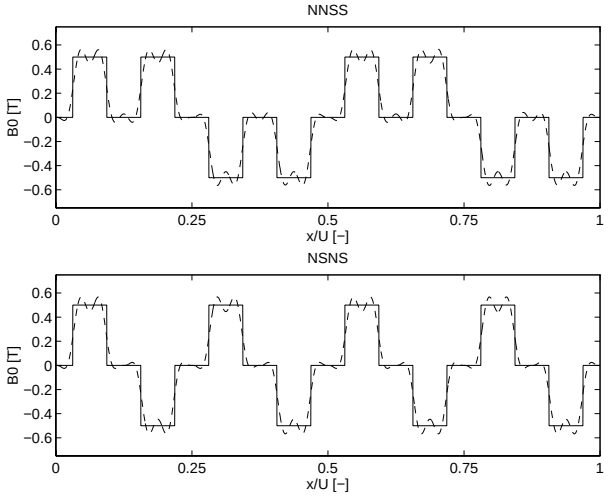

Figure 4: Approximated flux density $B_0(x)$ of a NNSS and a NSNS radial magnetic bearing configuration. Dashed line: approximated flux density using 30 harmonics, solid line: original flux density.

Comparing the two Fourier series in figure 3 it can be seen that the configurations NNSS and NSNS (see figure 4) have different harmonic flux density components A_n and B_n. The first component of the Fourier series for the configuration NSNS is of higher order than for the configuration NNSS. Therefore, it is often supposed that NNSS leads to smaller losses than NSNS but measurements [8] show the opposite behaviour. In [7] a simple model is presented which confirms the common meaning without calculating the magnetic fields and forces. On the other hand the Fourier series for the configuration NNSS has more harmonic components than the configuration NSNS. It is clear that the question as to which configuration leads to higher losses cannot be answered without an adequate model.

4 Magnetic Fields

In this chapter all calculations will be shown for one term $C\mathrm{e}^{ikx}$ of the harmonic components of the boundary conditions (see equation 4).

Maxwell's equations without time variant fields (i.e. $\partial \boldsymbol{B}/\partial t = 0$ and $\partial \boldsymbol{D}/\partial t = 0$) can be written as

$$\nabla \times \boldsymbol{E} = 0 \tag{5}$$

$$\nabla \times \boldsymbol{H} = \boldsymbol{J} \tag{6}$$

The material equation is:

$$\boldsymbol{B} = \mu \boldsymbol{H} = \mu_0 \mu_r \boldsymbol{H} \tag{7}$$

Ohm's law is given by:

$$\boldsymbol{J} = \sigma \left(\boldsymbol{E} + \boldsymbol{v} \times \boldsymbol{B} \right) \tag{8}$$

Equations 5 - 8 can be combined to second-order partial differential equations.

$$\frac{1}{\mu\sigma} \nabla^2 \boldsymbol{B} + \nabla \times (\boldsymbol{v} \times \boldsymbol{B}) = 0 \tag{9}$$

The flux density has components in x and y directions, the eddy currents are flowing in z direction and the conductive part is moving in x direction.

$$\boldsymbol{B} = \begin{pmatrix} B_x \\ B_y \\ 0 \end{pmatrix}, \boldsymbol{J} = \begin{pmatrix} 0 \\ 0 \\ J_z \end{pmatrix}, \boldsymbol{v} = \begin{pmatrix} v_x \\ 0 \\ 0 \end{pmatrix} \tag{10}$$

B_x, B_y and J_z are functions of x and y.

Combining equations 9 and 10 leads to:

$$\frac{\partial^2 B_x}{\partial x^2} + \frac{\partial^2 B_x}{\partial y^2} - \mu\sigma v_x \frac{\partial B_x}{\partial x} = 0 \tag{11}$$

$$\frac{\partial^2 B_y}{\partial x^2} + \frac{\partial^2 B_y}{\partial y^2} - \mu\sigma v_x \frac{\partial B_y}{\partial x} = 0 \tag{12}$$

When the solution for one direction of the flux density field is found, the flux density of the other direction can be derived from the relation $\nabla \cdot \boldsymbol{B} = 0$ (conservation of flux) which requires:

$$\frac{\partial B_x}{\partial x} + \frac{\partial B_y}{\partial y} = 0 \tag{13}$$

The magnetic flux density field is driven by the applied magnetic field density B_0. Hence, the solutions with the same travelling wave dependence on x are assumed and the flux density takes the form:

$$\boldsymbol{B}(x, y) = \tilde{\boldsymbol{B}}(y)\mathrm{e}^{ikx} \tag{14}$$

The equations 11 and 12 can be transformed to:

$$\frac{\partial^2 \tilde{B}_x}{\partial y^2} - q^2 \tilde{B}_x = 0 \tag{15}$$

$$\frac{\partial^2 \tilde{B}_y}{\partial y^2} - q^2 \tilde{B}_y = 0 \tag{16}$$

with $q = \sqrt{k^2 + k\sigma\mu v_x}$ and with the general solutions:

$$\tilde{B}_x = -\frac{q}{ik}\left(a\mathrm{e}^{qy} - b\mathrm{e}^{-qy}\right) \tag{17}$$

$$\tilde{B}_y = a\mathrm{e}^{qy} + b\mathrm{e}^{-qy} \tag{18}$$

The solution domain is divided into two regions: region 1 corresponding to the air gap where $\sigma = 0$ and therefore $q = k$ and region 2, the moving conducting medium.

For region 1 the solutions are:

$$B_{x1} = i\mathrm{e}^{ikx}\left(a_1\mathrm{e}^{ky} - b_1\mathrm{e}^{-ky}\right) \tag{19}$$

$$B_{y1} = \mathrm{e}^{ikx}\left(a_1\mathrm{e}^{ky} + b_1\mathrm{e}^{-ky}\right) \tag{20}$$

The depth of region 2 is assumed to be very large compared with the penetration depth δ (see equation 1). Therefore, it can be assumed that the field density is zero for $y \to \infty$.

$$B_{x2} = b_2\frac{q}{ik}\mathrm{e}^{ikx}\mathrm{e}^{-qy} \tag{21}$$

$$B_{y2} = b_2\mathrm{e}^{ikx}\mathrm{e}^{-qy} \tag{22}$$

The constants a_1, b_1 and b_2 can be calculated with the boundary conditions at $y = 0$ and $y = \Delta$. At $y = 0$ the boundary conditions depend on the applied flux density and at $y = \Delta$ the magnetic field values for both regions must be equal.

$$B_{y1}(y = 0) = C\mathrm{e}^{ikx} \tag{23}$$

$$B_{y1}(y = \Delta) = B_{y2}(y = \Delta) \tag{24}$$

$$B_{x1}(y = \Delta) = \frac{1}{\mu_r} B_{x2}(y = \Delta) \tag{25}$$

From equations 23 - 25 a_1, b_1 and b_2 can be calculated:

$$a_1 = C\left(1 - \frac{q}{\mu_r k}\right)\frac{\mathrm{e}^{-k\Delta}}{2\gamma} \quad (26)$$

$$b_1 = C\left(1 + \frac{q}{\mu_r k}\right)\frac{\mathrm{e}^{k\Delta}}{2\gamma} \quad (27)$$

$$b_2 = C\frac{\mathrm{e}^{q\Delta}}{\gamma} \quad (28)$$

with $\gamma = \cosh k\Delta + \frac{q}{\mu_r k}\sinh k\Delta$.

5 Forces and Losses

To calculate the forces acting on the conducting medium, Maxwell's stress tensor is used [4], [9].

$$F_x = -\frac{1}{\mu_0}\int_s B_x B_y \mathrm{d}a \quad (29)$$

$$F_y = -\frac{1}{2\mu_0}\int_s B_y^2 - B_x^2 \mathrm{d}a \quad (30)$$

s is any closed surface surrounding the conducting body. It is useful to choose the surface at $y = \Delta$ and to integrate x from 0 to 2π and z from 0 to b, where b is the length of the magnetic bearing (see figure 1).

$$F_x = \frac{ibU}{\mu_0}\sum_{n=1}^{\infty}\frac{C_n\overline{C}_n}{\gamma_n\overline{\gamma}_n}\frac{q_n - \overline{q}_n}{\mu_r k_n} \quad (31)$$

$$F_y = \frac{bU}{\mu_0}\sum_{n=1}^{\infty}\frac{C_n\overline{C}_n}{\gamma_n\overline{\gamma}_n}\frac{q_n\overline{q}_n - \mu_r^2 k_n^2}{\mu_r^2 k_n^2} \quad (32)$$

$\overline{C}_n$, $\overline{q}_n$ and $\overline{\gamma}_n$ are the conjugate complex values of C_n, q_n and γ. The subscript n refers to the n-th harmonic of the applied flux density series.

The losses P can be calculated with:

$$P = F_x v_x \quad (33)$$

Figure 5 shows the increase of the drag force F_x and the decrease of the levitational force F_y with increasing velocity v_x. Losses can be reduced with rotor materials which have a low conductivity σ and a high relative permeability μ_r. For small values (e.g. $\mu_r < 1000$) the drag force increases drastically. In figure 5 it can be seen that the configuration NSNS leads to a reduced increase of the drag force compared with the configuration NNSS. The relative difference of the losses of these two configurations is about 15% - 20%.

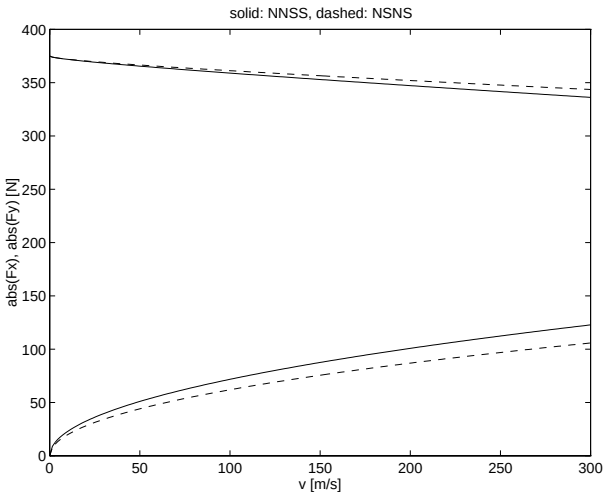

Figure 5: Upper curves: levitation force F_y, lower curves: drag force F_x.

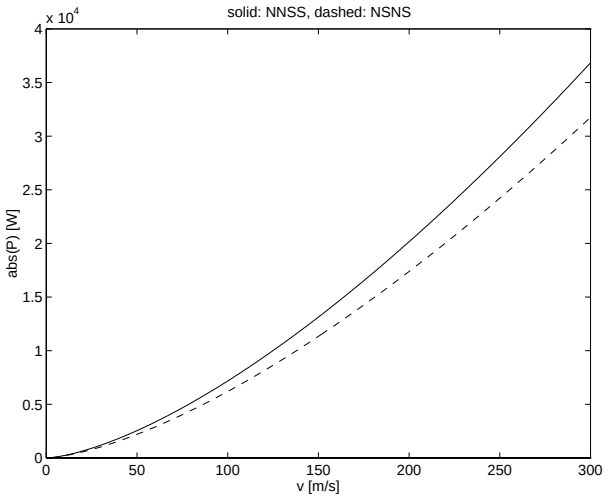

Figure 6: Losses P due to eddy currents inside the conducting and moving body.

6 Cross Coupling

In the previous chapter, the magnetic forces have been calculated for a simplified rectangular geometry of the rotor (see figure 2). This model is sufficient for the calculation of the forces of radial magnetic bearings when the flux density distribution in the bearing is symmetrical.

The forces calculated for the rectangular model can be transformed to the cylindrical model. The resulting levitation and drag forces acting on the rotor are zero but the drag forces lead to a resulting drag torque. When the rotor is excited the air gap and the flux density distribution are no longer symmetrical (see figure 7). When, for example, the flux density increases in one direction the flux density in the opposite direction must decrease due to the conservation of the flux. An excited rotor causes an asymmetrical flux density distribution which leads to differential forces. These forces cannot be calculated with equations 29 - 32 and, therefore, it is necessary to

transform the equations into the coordinate system of the rotor (see figure 1).

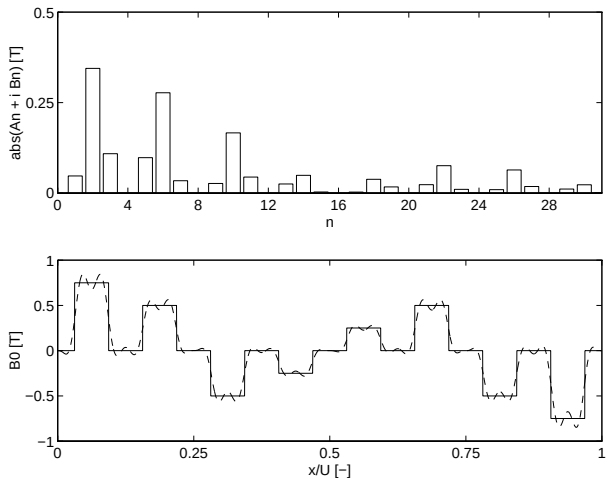

Figure 7: Differential flux excitation. Upper plot: Fourier series, lower plot: applied flux density.

$$F_x^* = \frac{1}{\mu_0}\int_s B_x B_y \sin(\varphi)\mathrm{d}a + \frac{1}{2\mu_0}\int_s \left(B_y^2 - B_x^2\right)\cos(\varphi)\mathrm{d}a \quad (34)$$

$$F_y^* = -\frac{1}{\mu_0}\int_s B_x B_y \cos(\varphi)\mathrm{d}a + \frac{1}{2\mu_0}\int_s \left(B_y^2 - B_x^2\right)\sin(\varphi)\mathrm{d}a \quad (35)$$

with $\varphi = 2\pi x/U = x/R$. The integrals of equation 34 and 35 can be solved in asimilar fashion to the calculations of the previous chapter. As mentioned before, an excitation of the rotor causes an asymmetrical flux density distribution. For correct calculations the variable air gap must be considered. The excited rotor geometry can be transformed with the Moebius-transformation into a new imaginary geometry system with two concentric circles. The partial differential equations 15 and 16 have to be transformed also. The additional distortion factors lead to equations which can only be solved by numerical methods. Numerical calculations show that the forces caused by the excited rotor are mainly caused by a change of the flux density distribution. The influence of the variable air gap is small and, therefore, it can be neglected (assuming $\Delta \ll U/16$). The simplified geometry shown in figure 2 will represent a system with a medium air gap.

$$F_x^* = \frac{bU}{2\mu_0}\sum_{n=1}^{\infty}\left(\frac{C_n\overline{C}_{n+1}}{\gamma_n\overline{\gamma}_{n+1}}\frac{\mu_r k_n + q_n}{\mu_r k_n}\frac{\mu_r k_{n+1} - \overline{q}_{n+1}}{\mu_r k_{n+1}} + \frac{C_{n+1}\overline{C}_n}{\gamma_{n+1}\overline{\gamma}_n}\frac{\mu_r k_{n+1} - q_{n+1}}{\mu_r k_{n+1}}\frac{\mu_r k_n + \overline{q}_n}{\mu_r k_n}\right) \quad (36)$$

$$F_y^* = \frac{ibU}{2\mu_0}\sum_{n=1}^{\infty}\left(\frac{C_n\overline{C}_{n+1}}{\gamma_n\overline{\gamma}_{n+1}}\frac{\mu_r k_n + q_n}{\mu_r k_n}\frac{\mu_r k_{n+1} - \overline{q}_{n+1}}{\mu_r k_{n+1}} - \frac{C_{n+1}\overline{C}_n}{\gamma_{n+1}\overline{\gamma}_n}\frac{\mu_r k_{n+1} - q_{n+1}}{\mu_r k_{n+1}}\frac{\mu_r k_n + \overline{q}_n}{\mu_r k_n}\right) \quad (37)$$

Figure 8 shows the basic behaviour of the forces F_x^* and F_y^* depending on the velocity v_x. The levitational force of a magnetic bearing decreases slowly with increasing speed. Contrary to the levitational force, the cross coupling force, which is zero at standstill, increases with increasing speed.

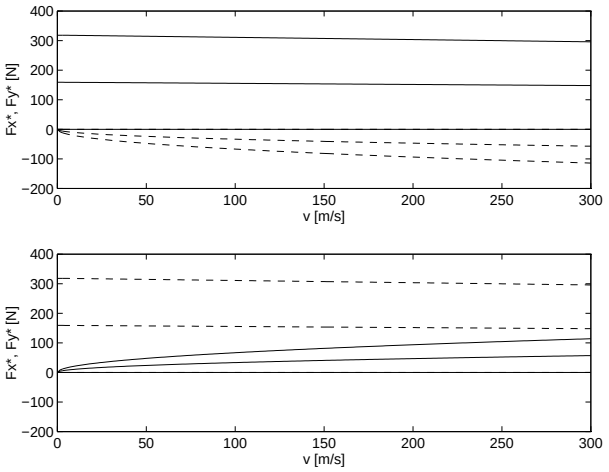

Figure 8: Differential magnetic bearing forces F_x^* (solid lines) and F_y^* (dashed lines). Upper plot: changing flux density distribution in x-direction, lower plot: changing flux density distribution in y-direction, steps : $\hat{B}_0, 1.5\hat{B}_0, 2\hat{B}_0$

7 Summary

This paper shows a model for eddy currents in an unlaminated rotor, rotating inside a radial magnetic bearing. Additionally to the levitational force, a drag force is acting on the rotor which leads to a retardation torque. When the rotor is excited the asymmetrical flux density distribution causes resulting forces in the x and y directions and, therefore, leads to a cross coupling. From the analytical solution for the flux density, all of these forces and the losses can be calculated. It is shown, that the configuration NSNS leads to lower losses than NNSS which corresponds with measurements in [8].

8 Outlook

Most rotors for magnetic bearing applications are laminated in order to reduce eddy currents. For some applications unlaminated rotors are used because the production costs are lower and the material strength is higher. The choice of the lamination thickness as well as its influence on the eddy current losses is an important design problem. It is astonishing that the simple geometry of laminated sheets leads to a difficult electromagnetic

problem (see also [9]). One approach to model the magnetic field of radial magnetic bearings with laminated sheets on the rotor is to use a time variant magnetic field. This approach is used for transformers but it cannot produce a drag force because the model consists neither of an eddy current flow nor a flux density distribution in the z direction. Another approach is a two dimensional Fourier approximation in the x and z directions. This model describes only the problem of an unlaminated rotor which is not infinite in length. Considering the edge effects of radial bearings, the calculated eddy current losses increase slightly whereas laminated rotors have much smaller losses. The assuptions of this model are only valid for large lamination thicknesses. Hence, this model cannot be used for laminated rotors. Both approaches cannot achieve an adequate model for laminated rotors when eddy currents are caused by moving conducting material under an applied time invariant magnetic field. It is unclear whether analytical solutions can be found for this problem.

References

[1] P. Allaire, R. Rockwell, and M. Kasarda. Magnetic and Electric Field Equations for Magnetic Bearing Applications. In *MAG '95 Magnetic Bearings, Magnetic Drives and Dry Gas Seals Conference & Exhibition*, Alexandria, 1995.

[2] K. Hebbale. *A Theoretical Model for the Study of Nonlinear Magnetic Dynamics*. PhD thesis, Cornell University, 1985.

[3] Institut für Elektrische Maschinen, ETH Eidgenössische Technische Hochschule, Zürich. *FEMAG Benutzeranleitung*, 1994.

[4] J. Jackson. *Klassische Elektrodynamik*. de Gruyter, Berlin, 1983.

[5] M. Kasarda, P. Allaire, E. Maslen, and G. Gillies. Design of a High Speed Rotating Loss Test Rig for Radial Magnetic Bearings. In *Fourth International Symposium on Magnetic Bearings*, Zurich, 1994.

[6] H. Marko. *Methoden der Systemtheorie*. Springer-Verlag, Berlin, 1986.

[7] F. Matsumura and K. Hatake. Relation between Magnetic Pole Arrangement and Magnetic Loss in Magnetic Bearing. In *3rd International Symposium on Magnetic Bearings*, Washington, 1992.

[8] T. Mizuno and T. Higuchi. Experimental Measurement of Rotational Losses in Magnetic Bearings. In *Fourth International Symposium on Magnetic Bearings*, Zurich, 1994.

[9] F. Moon. *Magneto-solid Mechanics*. John Wiley & Sons, New York, 1984.

[10] A. Sabnis. Analysis of Forces in Rectangular-Pole Geometries Using Numerical Integration Techniques. *IEEE Transactions on Magnetics*, 10, 3 1974.

[11] R. Stoll. *The analysis of eddy currents*. Clarendon Press, Oxford, 1974.

[12] H. Vullings. *Analytische Berekening van Elektromagnetische Velden en Krachten*. Technical report, TU Delft, 1992.

[13] S. Yamamura and T. Ito. Analysis of Speed Characteristics of Attracting Magnet for Magnetic Levitation of Vehicles. *IEEE Transactions on Magnetics*, 11, September 1975.

[14] T. Yoshimoto. Eddy Current Effect in a Magnetic Bearing Model. *IEEE Transactions on Magnetics*, 19, September 1983.